JOURNAL OF APPLIED ELECTROCHEMISTRY 25 (1995) 1098–1104

Evaluation of low-temperature cryolite-based electrolytes for aluminium smelting

A. M. VECCHIO-SADUS, R. DORIN, E. J. FRAZER*

CSIRO Institute of Minerals, Energy and Construction, Division of Minerals, PO Box 124, Port Melbourne, Victoria 3207, Australia

Received 28 November 1994; revised 28 February 1995

Aluminium was smelted in a laboratory-scale cell at temperatures down to 850 °C from cryolite-based electrolytes with bath ratios in the range 0.75–1.50. Electrolyses were conducted for 1–2 h using a current density of 1 A cm^{-2} on 5 cm^2 electrodes with an anode–cathode distance of 2 cm. Current efficiencies of up to 95% were recorded. In low bath ratio electrolytes, operation at alumina concentrations of $\geqslant 3$ wt % sometimes resulted in the aluminium deposit breaking into globules which clustered around the cathode. Under constant current conditions, the critical alumina concentration for the onset of anode effect was found to be ~2 wt %. The bubble evolution characteristics (i.e., size and frequency) which affect mass transfer and cell voltage were also evaluated. Overall, low-temperature cryolite-based electrolytes may offer a viable alternative to conventional compositions for aluminium smelting.

1. Introduction

The imminent introduction of wettable cathode technology by the aluminium industry will result in a substantial improvement to the energy efficiency of the smelting process. This technology allows operation at smaller anode–cathode distances (ACD) and hence, reduces power losses through the electrolyte. The development and implementation of low-temperature electrolytes (LTE) would further reduce energy consumption by decreasing the thermal demand of smelting cells. Low temperature smelting may also increase cathode life by reducing the rate of the thermal degradation processes. Additionally, the prospects for the development and introduction of inert anodes would be enhanced.

The impact of lowering the operating temperature through modified electrolyte composition has been studied by many authors (e.g. [1–6]). The anticipated benefits include an improved current efficiency (CE) and reduced anode carbon consumption. However, the effects of lower alumina solubility, electrolyte conductivity, and density differential between metal and electrolyte, will have to be addressed in any application. Sleppy and Cochran [6] reported CEs of ~90% in electrolytes with bath ratios (BR = wt NaF/wt AlF_3) 0.65–0.80 operating at 730–900 °C. However, a solid cryolite 'crust' formed on the cathode surface unless the electrolyte temperature was maintained at ~100 °C above the liquidus temperature of the bulk NaF–AlF_3 composition.

The cryolite-based electrolyte in modern aluminium smelting cells typically contains 2–4 wt % alumina, 8–13 wt % aluminium fluoride, 3–7 wt % calcium fluoride, 1.5–3 wt % lithium fluoride and 2–4 wt % magnesium fluoride [7]. Most industrial electrolytes operate with BRs in the range 1.15–1.35 and cell temperatures between 940 and 980 °C. Aluminium fluoride is the most commonly used additive to lower melting point, with up to ~30% AlF_3 in excess of the cryolite composition allowing operation between 850–900 °C. Although AlF_3 and CaF_2 decrease aluminium metal solubility, they also decrease alumina solubility and electrical conductivity. LiF can be used to compensate for the losses in conductivity at high AlF_3 concentrations [8].

In previous work [9, 10] it was demonstrated how parameters relevant to aluminium smelting could be determined in a novel laboratory-scale cell with a wettable cathode. The present paper reports on the use of this cell for the evaluation of several LTEs based on additions of AlF_3. Measurements were made of CE, and of the influence of alumina concentration on the onset of the anode effect and the stability of the aluminium metal film. Additionally, the effects of electrolyte composition on anode gas evolution characteristics were studied.

2. Experimental details

2.1. *Electrochemical cell*

The multi-element graphite electrochemical cell and Inconel furnace used in this work have been described previously [9, 10]. An argon atmosphere was maintained within the furnace to prevent excessive oxidation of the graphite cell components. As before, the molybdenum cathode (Metallwerk Plansee GmbH, 99.95%; diam. 25 mm) was constructed with a 5° conical concave cross-section (i.e., 170° included angle).

* Author to whom correspondence should be addressed.

0021-891X

Table 1. Summary of electrolyte compositions and operating temperatures

*Composition**	*xs-AlF_3*† /%	*Al_2O_3* /wt%	*CaF_2* /wt%	*BR*	*$T_{oper.}$* /°C
LTE 1	0–30	satd	0	1.50–0.86	975–884
LTE 2	15–38	4	5	1.09–0.77	966–850
LTE 3	15–30	satd	5	1.09–0.86	948–890
LTE 4	25–30	4	0	0.92–0.86	923–892

* LTE 5 (4 wt% Al_2O_3, BR 0.75, $T_{oper.}$ 850 °C).
† Defined as the mass percent of AlF_3 in excess of the Na_3AlF_6 composition.

This substrate material allows the formation of a stable aluminium film and recovery of the aluminium product for CE calculation and for analysis. During a standard experiment producing ~2 g aluminium, the maximum thickness of the slightly domed deposit was ~3 mm.

Anodes were fabricated from graphite rod (Morganite EY941; diam. 24 mm) and sheathed with recrystallized alumina tubing (Alsint, 99.7%) to define the active surface area of ~5 cm^2; a 1.5 mm thick section was left exposed to allow for consumption during electrolysis. The horizontal working face had a complementary 5° conical cross-section to the cathode. Additionally, the anode was fitted with an alumina sleeve (44 mm o.d. × 34 mm i.d.) to give an anode-sleeve gap of 5 mm. The bottom of the sleeve was set 15 mm below the anode surface and positioned with a clearance of 5 mm above the base of the cell, to give an ACD of 2 cm (see [10], Fig. 2).

For the study of anode effects, anodes without alumina sleeves were sheathed with boron nitride (Union Carbide, HBR grade) and were fabricated with an additional 1 mm of exposed graphite to allow for the extra consumption over longer electrolysis periods (total area ~5.5 cm^2). Boron nitride was used as the sheath material since the recrystallized alumina tubing was found to dissolve significantly in electrolytes with low alumina concentrations. To test the effect of extremes of anode geometry on bubble characteristics, two unsleeved graphite anodes (diam. 24 mm), one with a horizontal surface (total area ~5 cm^2) and the other domed in shape (total area 7.6 cm^2) were constructed and sheathed with boron nitride. Again, the above experiments were run at a nominal ACD of 2 cm.

2.2. *Electrolyte composition*

Synthetic cryolite and alumina (supplied by Comalco Research Centre, Australia), aluminium fluoride (CERAC Inc., 99.9%) and calcium fluoride (Aldrich, 99.9%) were vacuum dried at 120 °C for 4 h and then stored *in vacuo* until required. In the preparation of the electrolyte (total weight, 300 g), the weight of alumina added was adjusted to allow for the residual level in the cryolite (~2 wt%). Bath ratios for LTEs were selected in the range 0.75–1.09 to give liquidus temperatures between 811 and 956 °C (calculated from [7, 8]). Experiments were normally run at a 10 °C superheat (i.e., the difference between the operating temperature and the calculated liquidus). A summary of electrolyte compositions and operating temperatures is given in Table 1.

2.3. *Electrochemical and mass transfer measurements*

Aluminium was normally electrodeposited at a current density of ~1.0 A cm^{-2} for 24 000 coulombs (5 A, 80 min) using a 5 A capacity constant-current power supply [9, 10]. The cell voltage and resistance were continuously monitored on a Yokogawa HR1300 hybrid recorder. In addition, experiments were run for 17 030 coulombs to examine aluminium film stability and for up to 37 000 coulombs to study anode effects. Current efficiencies were determined from the weight of the aluminium product and Faraday's law; the weight of aluminium was corrected for the molybdenum dissolved from the cathode substrate (up to 10 wt% at 975 °C). The weight of the aluminium deposit obtained under the same conditions was reproducible to ±0.5%; no correction for the electrolytic co-deposition of sodium (usually <0.7 wt%) was made.

Mass transfer measurements involved additions to the electrolyte (~0.01 wt%) of the metal tracers, copper oxide (BDH, Analar) and manganese fluoride (BDH, LR). The aluminium product was analyzed for co-deposited copper and manganese by atomic absorption spectroscopy and the mass transfer coefficient for aluminium was calculated as before [9–11].

Bubble characteristics were studied using digital analysis of fluctuations in cell voltage and resistance. The collection and analysis of data have been described previously [9, 10].

3. Results and discussion

3.1. *Effect of bath ratio on current efficiency*

Current efficiencies were determined over the BR range 0.86–1.50 in LTE 1 and the results are presented in Fig. 1. A decrease in CE from a maximum of 88% to 76% was observed as the BR increased from 1.00 to 1.50; the decrease was linear over the range 1.00–1.41. This decrease is expected because of the corresponding increase in aluminium metal solubility and operating temperature. Using an average value for the dependence of CE on operating temperature of ~0.2%/°C derived from [12], then the observed change in CE with BR is ~10%/unit BR, which is a comparable slope to literature data [13]. At BRs < 0.92 there was a rapid decrease in CE combined with the formation of aluminium globules (~25% of total mass) at the cathode rather than a coherent metal film. At BR 0.86, the entire aluminium deposit was recovered in globular form. The formation of globules may increase aluminium losses via dispersion and dissolution and hence, lower CE. The

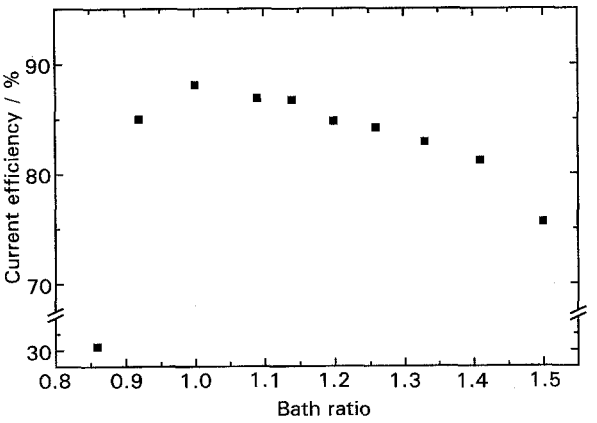

Fig. 1. Effect of BR on CE for composition LTE 1 (satd Al_2O_3, nil CaF_2).

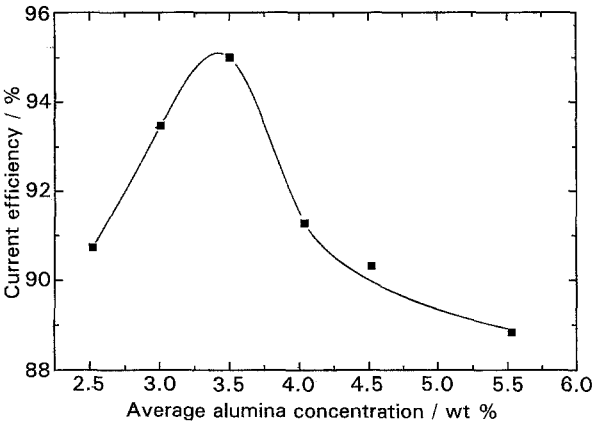

Fig. 2. CE as a function of average alumina concentration for LTE 5 at BR 0.75 and 850 °C.

formation of aluminium droplets has been observed by Beck [14, 15] at BR 0.64.

Current efficiency was also affected by changing the alumina concentration from saturated to 4 wt % and adding CaF_2, such as in LTE 2 where CEs of ~90% were obtained over the BR range 0.86–1.09. Although some metal globules (~20% of total mass) were formed at BRs $\leqslant$ 0.92, a sharp decrease in CE (to ~80%) was observed only at BR 0.77 where the entire aluminium product was obtained as globules. In LTE 3, containing 5 wt % CaF_2 and saturated with alumina, a distinct increase in CE from ~86% to ~93% was observed with decreasing BR, which occurred even with the formation of globular aluminium at BRs $\leqslant$ 0.92. These latter values of CE can be attributed, in part, to a reduction in aluminium metal solubility caused by the addition of CaF_2 or CaF_2/saturated alumina. Certainly, lower CEs were observed in LTE 4 containing no CaF_2 and 4 wt % Al_2O_3 at BRs $\leqslant$ 0.92 (46% at BR 0.86, 84% at BR 0.92). Current efficiencies for composition LTE 5 at BR 0.75 were ~95% with only a small fraction of the aluminium product in globular form; this is similar to the results obtained by Sleppy and Cochran [6] over the BR range 0.65–0.80. Presumably, the superior performance of LTE 5 compared to LTE 4 can be accounted for by the reduction in BR, lower operating temperature and less globule formation.

In previous work using LTE 1 over a limited BR range (1.14–1.41) [10], a dependence of CE on mass transfer rate at the cathode was obtained because of the mutual dependence of these latter variables on BR. However, in the present study, since no dependence of mass transfer rate on BR was found, no dependence of CE on mass transfer rate could be inferred.

3.2. *Effect of alumina concentration on current efficiency*

Figure 2 shows that a maximum CE of ~95% was obtained at an average alumina concentration of 3.5 wt % for LTE 5. Since the experiments were conducted at fixed BR *and* fixed temperature, the fall in CE in the range 3.5–5.5 wt % alumina can only be accounted for by globule formation (up to 100% of the deposit; see Section 3.4.). The increase in CE of ~4% in moving from 2.5 to 3.5 wt % alumina is unexpected since this change is much larger than literature values of $\leqslant$ 1.5% CE/wt % alumina (see [16] for a summary). At this stage, no satisfactory explanation for this behaviour can be advanced.

3.3. *Effect of bath ratio on cell resistance*

The conductivity of the electrolyte is an important factor in determining cell performance because it controls the ohmic voltage drop through the electrolyte. Increasing AlF_3 concentrations (i.e., >12 wt %) and decreasing operating temperatures lower the electrolyte conductivity. For a BR 0.74 electrolyte containing 3 wt % alumina, Sleppy and Cochran [6] reported a ~10% increase in electrical conductivity per 100 °C. In LTE 5, which contained a very high AlF_3 concentration and was operated at 850 °C, an increase in cell voltage and resistance (10–15%) was evident compared with LTEs 1 and 2.

A plot of the observed and theoretical cell resistance at an electrolysis time of 20 min against BR (0.86–1.20) for LTE 1 is shown in Fig. 3; similar behaviour was observed for LTE 3. The theoretical electrolyte resistance was calculated from the conductivities of the various compositions [17], assuming that the current path was restricted to the cylindrical channel between the anode and cathode. As expected, the observed values were less than the theoretical because the actual current path between the electrodes was non-cylindrical (i.e., a fanning effect). In addition, the observed trend in resistance with BR had an opposite slope to the theoretical line. This could be partly attributed to an increase in the overall conductivity caused by an increase in the concentration of dissolved aluminium metal as the BR was increased [18]. However, in composition LTE 2 (with 4 wt % Al_2O_3), both the observed and theoretical resistance against BR relationships had parallel slopes of similar magnitude. It is of interest to note that the two electrolytes which gave opposing slopes for the theoretical and measured resistance (i.e., LTEs 1 and 3) were both

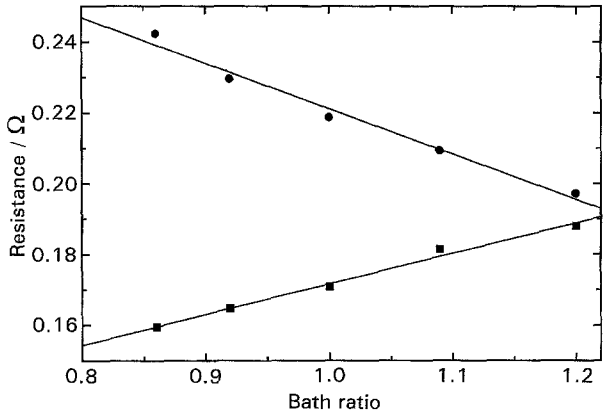

Fig. 3. Plot of the observed (at 20 min) and theoretical resistance against BR for LTE 1 (satd Al_2O_3, nil CaF_2); (■) experimental; (●) theoretical.

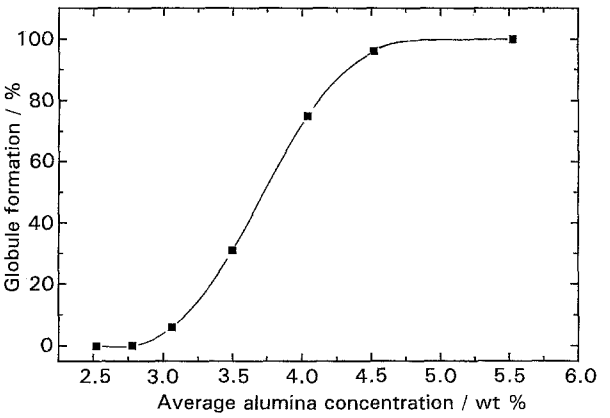

Fig. 4. Percentage of globule formation as a function of average alumina concentration for LTE 5 at BR 0.75 and 850 °C.

alumina saturated. This suggests that factors other than the electrolyte conductivity, such as the characteristics of anode bubble evolution (i.e., size, coverage and layer thickness), may also be important in determining cell resistance in high alumina electrolytes.

3.4. *Metal film stability*

As noted in Section 3.1, under certain conditions, a proportion of the aluminium metal product was recovered as discrete globules (diam. 0.5–10 mm) clustered around the cathode rather than a coherent metal film. Globule formation appeared to be related to a combination of low BR and high alumina concentration. To confirm that globule formation did not occur in the post-electrolysis pre-freezing period, that is, was not an artefact of the experimental procedure, some electrolytes were allowed to freeze while maintaining the electrolysis current. At an average alumina concentration of ~3 wt %, the percentage of globules did not vary significantly from the normal experimental procedure.

The effect of alumina concentration on globule formation was determined by carrying out electrolyses over selected narrow ranges of alumina concentration in LTE 5. The percentage of product formed as globules was estimated from the ratio of mass of globules to total metal recovered. Figure 4 illustrates that the percentage of globules in the deposit was *always* zero at an average alumina concentration $\leqslant 2.75$ wt %, increasing to virtually 100% globules in moving from 3 to 5 wt % average alumina. Since there is little variation in the calculated aluminium–electrolyte density difference over the working range of alumina concentration [19], the change in film behaviour observed at ~3 wt % alumina implies a decrease in the interfacial tension at the aluminium–electrolyte boundary. However, Utigard and Toguri [20] have shown that, in conventional electrolytes, interfacial tension increases with increasing alumina concentration (by decreasing sodium activity at the boundary), and this would tend to stabilize the interface.

It has been shown [6] that a change in the AlF_3 content of the electrolyte could cause precipitation of cryolite on the aluminium surface, and this could change the interfacial tension. However, it is unlikely that such precipitation is related to the change in alumina concentration or occurs over the short time scale of the present experiments. In addition, it has recently been reported [21] that alumina may be soluble only up to 2 wt % in electrolytes with compositions similar to LTE 5. This suggests that undissolved alumina may be present at the higher nominal concentrations used here. It may be possible that the microdroplets of aluminium at the cathode surface are acting as nuclei for the precipitation of alumina from a (super)saturated electrolyte. Indeed, Thonstad and Liu [22] have reported that particles of undissolved alumina can accumulate at the interface between liquid aluminium and the electrolyte.

The occurrence of globule formation in industrial cells would need to be confirmed because there may be differences in aluminium film thickness and in the wetting behaviour of other cathode substrates (e.g., TiB_2/carbon composite or carbon) by aluminium, which may modify the behaviour observed in the present laboratory-scale cell.

3.5. *Bubble evolution characteristics*

3.5.1. Dominant bubble frequency and mean bubble radius. In previous work in LTE 1 over a limited BR range (1.14–1.50), no dependence of dominant bubble frequency and mean bubble radius (for method of calculation see [9]) on BR was observed [10]. Here, however, at low BRs, LTEs 1–3 all exhibited a dependence of dominant bubble frequency on BR. The plot for LTE 1 at an electrolysis time of 60 min (Fig. 5) shows a threefold increase in frequency over the BR range 0.86–1.50. The corresponding plots at 20 min for compositions LTE 1 and 2 showed similar behaviour. In LTE 1, a decrease in mean bubble radius with increasing bubble frequency was observed (Fig. 6). The decrease in calculated mean bubble volume was compensated for by the increase in bubble frequency, suggesting that there was no significant change in gas hold-up (volume retained in the gas bubble layer) over the range of BR. The data for

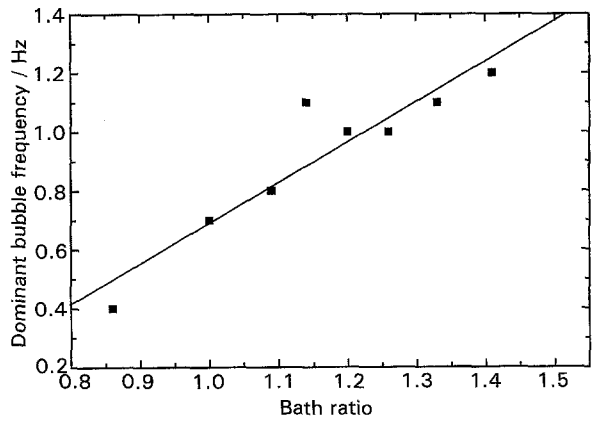

Fig. 5. Dependence of dominant bubble frequency at 60 min on BR for LTE 1 (satd Al_2O_3, nil CaF_2).

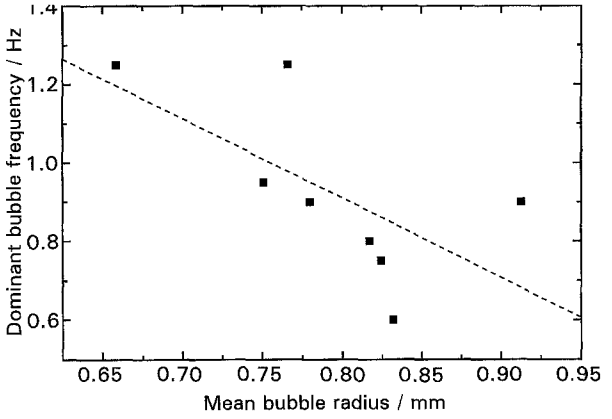

Fig. 6. Variation of dominant bubble frequency with mean bubble radius at 20 min for LTE 1 (satd Al_2O_3, nil CaF_2). Dashes show line of best fit.

LTE 5 at BR 0.75 over a range of alumina concentration, showed a similar trend to LTE 1. Again, the decrease in calculated bubble volume was compensated for by an increase in bubble frequency. Note that this analysis assumes that the *dominant* bubble frequency is strongly correlated to bubble *detachment* events rather than *coalescence* events.

In contrast to LTE 1, there was no systematic dependence of mean bubble radius on BR or on bubble frequency for LTEs 2 and 3, which both contain CaF_2. Since all the experiments were conducted at constant current, the rate of gas evolution was also constant assuming similar anodic CEs. Therefore, there could be an increase in gas hold-up with decreasing BR for these LTE compositions.

3.5.2. Effect of anode geometry on bubble characteristics. Table 2 summarizes the changes observed in bubble characteristics with extremes of anode geometry in LTE 5. Overall, there was a decrease in mean bubble radius and an increase in dominant bubble frequency as the inclination of the anode was changed from horizontal to domed. A similar trend in bubble radius with change in geometry was observed previously [9] in an electrolyte with BR 1.50 at 960 °C. Interestingly, in this case, the bubble evolution frequency on the 5° anode was bimodal at longer electrolysis times. The formation of smaller bubbles on the domed anode can be partly accounted for by the lower operating current density. The degree of coalescence on the horizontal surface was greater than on the conical surface, as evidenced by the formation of larger bubbles with little change in dominant bubble evolution frequency. This situation would be expected to result in increased gas hold-up and a higher cell resistance for the horizontal geometry.

3.6. *Anode effects*

The anode effect is detrimental because it leads to an increase in energy consumption, fluoride emissions, electrolyte temperature and sidewall attack [23]. Therefore, the alumina concentration range where anode effects are likely to occur was investigated here. Electrolytes with composition LTE 5 at an initial concentration of 3 wt % alumina were electrolysed at constant current until the anode effect stopped the current flow. The anode was then rotated to re-establish supply of the electroactive species to the anode and the electrolysis continued. The total charge passed at each stage was recorded to allow calculation of the theoretical amount of alumina consumed, and hence, the average alumina remaining in the electrolyte; this is the critical alumina concentration for anode effect. A plot of critical alumina concentration against the square root of the anode rotation rate is shown in Fig. 7. The anode effect initially occurred at ~2 wt % alumina in the absence of rotation, the convection being driven by gas evolution only. A linear decrease in critical alumina concentration was observed as the rotation rate was increased, dropping to ~1 wt % at 1500 rpm. The critical alumina concentration obtained here without forced convection is comparable to that observed in industrial cells [24]. One would not expect anode effects to occur at $\geqslant$2 wt % alumina using this electrolyte composition in industrial cells, since convection is controlled by both gas evolution *and* magnetohydrodynamic effects.

Table 2. Changes in bubble characteristics with anode geometry in LTE 5

Anode geometry	*Mean bubble radius at 20 min* /mm	*Mean bubble radius at 60 min* /mm	*Dominant bubble frequency at 20 min* /Hz	*Dominant bubble frequency at 60 min* /Hz
Horizontal	1.67	1.31	0.30	0.5
5° conical	0.76	0.51	0.25	0.25, 0.9
Domed	0.44	0.25	1.60	1.0–2.5

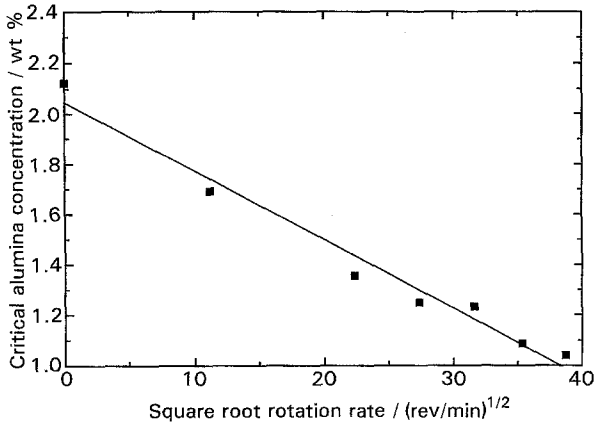

Fig. 7. Plot of critical alumina concentration against the square root of anode rotation rate for LTE 5 at BR 0.75 and 850 °C.

3.7. *Anode consumption*

Examination of frozen electrolytes from experiments using LTE 5 revealed apparently higher levels of graphite dusting compared with other compositions. Therefore, anode carbon consumption was monitored over six electrolyses by measuring anode weight loss. The average excess carbon consumption was estimated to be $6.7 \pm 3.6\%$; the stoichiometric value was determined from the calculated CO/CO_2 ratio for the measured CE via the Pearson–Waddington equation [25]. This amount represents physical carbon losses and is similar to values quoted for laboratory and industrial cells [26]. Therefore, since the anode carbon consumption via electrolysis in LTE 5 cannot be considered excessive, there may have been additional dusting from the unprotected graphite inner liner of the cell. Certainly, it has been reported [6] that graphite above the electrolyte level is attacked, perhaps by $NaAlF_4$ vapour.

4. Conclusions

Aluminium has been successfully smelted in a laboratory-scale cell from cryolite-based electrolytes operating as low as 850 °C. Current efficiencies up to 95% were normally obtained from electrolytes containing high concentrations of aluminium fluoride with BRs as low as 0.75. Under constant current conditions, anode effects were observed at critical alumina concentrations comparable with values usually obtained in industrial cells. Compared with conventional electrolytes, increases in cell voltage and resistance were obtained with decreasing BR and temperature.

The dominant bubble frequency, in general, was dependent on BR, with up to a threefold increase in frequency over the BR range studied for LTE 1. Little change in gas hold-up is anticipated in this electrolyte as BR is reduced. No dependence of mean bubble radius on BR or on dominant bubble frequency was found in compositions LTE 2 and LTE 3, and this could suggest an increase in gas hold-up with decreasing BR in these two compositions.

The form of the aluminium deposit obtained was strongly dependent upon BR and alumina concentration. The aluminium film broke into globules at low BR ($\leqslant 0.92$) and high alumina concentrations ($\geqslant 3$ wt %), and this phenomenon was sometimes linked with a decrease in CE. Therefore, the successful application of cryolite-based LTEs to industrial cells incorporating wettable cathodes may depend upon the physical stability of the aluminium surface, particularly at high alumina concentrations. Since any localized increase in alumina concentration may cause metal film instability, feed control will be a major operational consideration.

Acknowledgements

We acknowledge the assistance of J. F. Kubacki for the construction of cell components, and P. M. Hoobin and C. McInnes for analytical services. We also thank K. J. Cathro, D. C. Constable and R. S. Stojanovic for comments on the manuscript. We acknowledge Comalco Research Centre, Victoria, Australia for the supply of electrolyte materials.

References

[1] N. E. Richards, *in* 'Bayer and Hall–Héroult process—selected topics' (edited by K. Bielfeldt and K. Grjotheim), Aluminium-Verlag, Düsseldorf (1988) pp. 115–119.
[2] N. E. Richards, *in* Proceedings of the Savard/Lee International Symposium on Bath Smelting (edited by J. K. Brimacombe, P. J. Mackey, G. J. W. Kor, C. Bickert and M. G. Ranade), The Minerals, Metals and Materials Society, Warrendale, USA (1992) pp. 67–82.
[3] K. Grjotheim and H. Kvande, 'Introduction to aluminium electrolysis: understanding the Hall–Héroult process', 2nd ed., Aluminium-Verlag, Düsseldorf (1993) p. 51.
[4] A. T. Tabereaux, T. R. Alcorn and L. Trembley, *in* 'Light Metals 1993' (edited by S. K. Das), The Minerals, Metals and Materials Society, Warrendale, USA (1993) pp. 221–226.
[5] Z. Qiu, M. He and Q. Li, *Trans. NFsoc.* **3** (1993) 11.
[6] W. C. Sleppy and C. N. Cochran, *in* 'Light Metals 1979' (edited by W. S. Peterson), The Metallurgical Society of AIME, USA (1979) pp. 385–395.
[7] K. Grjotheim and H. Kvande, *op. cit.* [3], p. 48.
[8] W. Haupin, *JOM* **43** (1991) 28.
[9] R. Dorin and E. J. Frazer, *J. Appl. Electrochem.* **23** (1993) 933.
[10] R. Dorin, E. J. Frazer and A. M. Vecchio-Sadus, *in* 'Light Metals 1994' (edited by U. Mannweiler), The Minerals, Metals and Materials Society, Warrendale, USA (1994) pp. 205–210.
[11] V. A. Ettel, B. V. Tilak and A. S. Gendron, *J. Electrochem. Soc.* **121** (1974) 867.
[12] K. Grjotheim, C. Krohn, M. Malinovský, K. Matiašovský and J. Thonstad, 'Aluminium electrolysis: fundamentals of the Hall–Héroult process', 2nd ed., Aluminium-Verlag, Düsseldorf (1982) p. 339.
[13] K. Grjotheim, C. Krohn, M. Malinovský, K. Matiašovský and J. Thonstad, *op. cit.* [12], p. 342.
[14] T. R. Beck, *in* 'Light Metals 1994' (edited by U. Mannweiler), The Minerals, Metals and Materials Society, Warrendale, USA (1994) pp. 417–423.
[15] T. R. Beck, Electrochemical Technology Corp. Report DOE/CE/15433-T3 DE92 015723, 15 June 1992.
[16] P. A. Solli, T. Haarberg, T. Eggen, E. Skybakmoen and A. Sterten, *in* 'Light Metals 1994' (edited by U. Mannweiler), The Minerals, Metals and Materials Society, Warrendale, USA (1994) pp. 195–203.
[17] P. Fellner, S. Midtlyng, Å. Sterten and J. Thonstad, *J. Appl. Electrochem.* **23** (1993) 78.
[18] A. N. Baraboshkin, *Melts* **7** (1993) 214.

[19] T. A. Utigard, *Can. Met. Quart.* **32** (1993) 327.
[20] T. Utigard and J. M. Toguri, *Met. Trans. B* **16B** (1985) 333.
[21] M. Somerville and S. Jahanshahi, *in* Proceedings of the Second Australian Melt Chemistry Symposium, G. K. Williams CRC, Melbourne, Australia (1995) pp. 5–9.
[22] J. Thonstad and Y. Liu, *in* 'Light Metals 1981' (edited by G. M. Bell), The Metallurgical Society of AIME, USA (1981) pp. 303–312.
[23] K. Grjotheim and H. Kvande, *op. cit.* [3], pp. 210–212.
[24] E. W. Dewing, *Can. Met. Quart.* **30** (1991) 153.
[25] T. G. Pearson and J. Waddington, *Disc. Faraday Soc.* **1** (1947) 307.
[26] K. Grjotheim, C. Krohn, M. Malinovský, K. Matiašovský and J. Thonstad, *op. cit.* [12], pp. 228–233.